Semicarbonized Subwavelength-Nanopore-Structured Nanocellulose Paper for Application in Solar Thermal Heating

*Thanakorn Yeamsuksawat, Yoshitaka Morishita, Jun Shirahama, Yintong Huang, Takaaki Kasuga, Masaya Nogi, Hirotaka Koga**

SANKEN (The Institute of Scientific and Industrial Research), Osaka University, 8-1 Mihogaoka, Ibaraki, Osaka 567-0047, Japan

ABSTRACT

Recently, there has been remarkable progress in solar thermal heating by applying biomass-derived carbons, which can absorb and convert solar light into thermal energy. The design of subwavelength nanoporous and molecular structures of biomass-derived carbons is required for suppressed reflection and enhanced absorption of solar light. However, such designs are difficult because conventional biomass-derived carbons exhibit intrinsic microstructures and are prepared under specific carbonization conditions. In this study, a wood cellulose nanofiber-derived carbon is proposed to tailor both subwavelength nanoporous and molecular structures. Cellulose nanofibers are first constructed into a paper, denoted as “nanopaper”, exhibiting subwavelength

nanoporous structures by tailoring the pore spaces between cellulose nanofibers. The as-prepared nanopaper is then carbonized at various controlled temperatures to tailor the cellulose molecular structure, *i.e.*, grow graphitic carbon domains. The graphitic carbon domains grown by semicarbonization at 500 °C adequately balance solar absorption and reflection, while the subwavelength nanoporous structures suppress solar reflection. Thus, the semicarbonized nanopaper with tailored nanoporous and molecular structures exhibits superior solar thermal heating to competitive nanocarbons, also affording thermoelectric power generation. This study can guide the structural and functional design of bionanocarbons for solar thermal heating.

INTRODUCTION

Biomass-derived carbon materials have recently attracted increased interest owing to their unique physical and chemical properties, intrinsic high-specific-surface-area porous structures, and sustainability.[1,2] The potential applications of biomass-derived carbon materials include adsorption,[3] separation,[4] sensing,[5,6] energy storage,[7,8] and photothermal heating,[9] among which photothermal heating has recently garnered the most attention for converting renewable solar light energy into heat.[10–15] Photothermal heating is achieved using photothermal materials that enable light to be absorbed and then converted into heat. Biomass-derived carbons are promising photothermal materials because carbon materials absorb light over a broader wavelength range (approximately 300–2500 nm) than other materials like plasmonic metal nanoparticles (approximately 300–1000 nm) and metal oxide semiconductors (approximately 300–1500 nm),[16] which is beneficial for absorbing solar light in the wavelength range of 300–

2500 nm (The American Society for Testing and Materials (ASTM) G173-03, Air Mass 1.5 Global spectrum (AM1.5G))[17].

To use solar light energy more efficiently, photothermal materials must be structurally and functionally designed to improve their solar thermal heating performances.[16] For example, subwavelength nanoporous structures have been extensively tailored for application as plasmonic metal nanoparticles and metal oxide semiconductors to enhance light absorption by suppressing light reflection to the outer surface, which is known as "light confinement."[18] For carbon-based photothermal materials, their sp^2-hybridized carbon-based molecular structures, such as the distribution of the highest occupied molecular orbital (HOMO) and the lowest unoccupied molecular orbital (LUMO), must also be designed because they not only affect the light-absorption wavelength range but also convert absorbed light into heat via vibrational relaxation.[19] Therefore, tailoring both the subwavelength nanoporous and molecular structures of biomass-derived carbon materials would be a rational strategy to optimize solar thermal heating.

Recently, various biomass-derived carbon materials, such as carbonized wood,[10] cotton,[11] mushroom,[12] sugarcane,[13] daikon,[14] and agave flower stalk,[15] have been reported for solar thermal applications. Because these natural biomass materials inherently exhibit microstructures, their carbonized derivatives also intrinsically exhibit them, thereby hindering the design of subwavelength nanoporous structures. These biomass materials are carbonized to form sp^2-hybridized carbon-based molecular structures, thereby decreasing the HOMO-LUMO bandgap (such as the π–π^* energy gap) and thus absorbing light over a broad wavelength range. In previous studies, however, these molecular structures have not been tailored to optimize solar light absorption yet because the materials are frequently carbonized under specific conditions. In other words, the impact of carbonization conditions on the solar light absorption of the

carbonized biomass materials has been insufficiently investigated. Thus, the design of biomass-derived carbon materials exhibiting nanoporous and molecular structures desirable for solar thermal heating applications has proven difficult.

Herein, a cellulose nanofiber-derived carbon material exhibiting tailored nanoporous and molecular structures is proposed for effective solar thermal heating. Cellulose nanofiber, which is mainly extracted from wood cell walls, has attracted significant attention as a fascinating biomass nanomaterial because of its excellent physical properties, nanostructures, abundance, and sustainability.[20–22] At present, cellulose nanofibers can be produced in a large-scale industrial operation, and its market is estimated to reach USD 963 million by 2026.[23] Cellulose nanofibers can be used as a building block to fabricate nanostructures because of its nanofiber morphology. Moreover, because the cellulose sp^3-hybridized carbon structure contains high oxygen and hydrogen contents,[24] carbonization can be used to tune cellulose nanofiber molecular structures over a wide range.[25] Carbonized cellulose nanofiber materials have been reported for adsorption and electronic applications.[25–28] To our best knowledge, however, the tailoring nanoporous and molecular structures of carbonized cellulose nanofiber materials for their application in solar thermal heating has been unexplored. In this study, cellulose nanofibers are fabricated into a paper (hereafter denoted as "nanopaper"), exhibiting nanoporous structures by tailoring the pore spaces between cellulose nanofibers and is subsequently carbonized at controlled temperatures to gradually grow sp^2-hybridized carbon domains (**Figure 1**). The carbonized nanopaper, fabricated with the as-tailored nanoporous and molecular structures, exhibits excellent solar thermal heating performance, which is superior even to the competitive nanocarbon materials such as carbon nanotube (CNT) and graphene films.

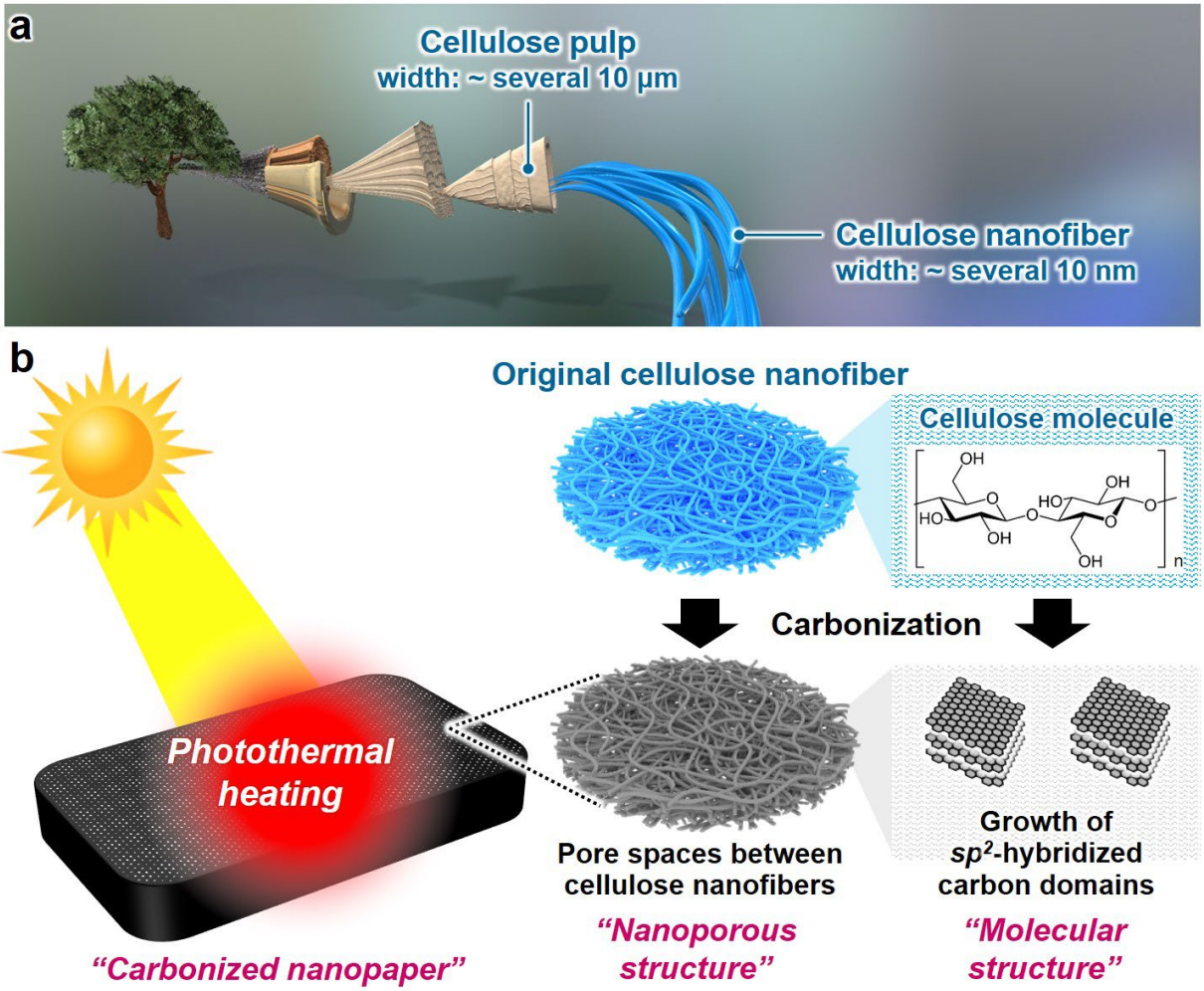

Figure 1. Schematic illustrating the design strategy used in this study. (a) Hierarchical structure from wood to cellulose pulp and cellulose nanofiber, and (b) photothermal heating by irradiating carbonized cellulose nanofiber paper (*i.e.*, nanopaper) exhibiting tailored nanoporous and molecular structures.

RESULTS AND DISCUSSION

Tailoring carbonized nanopaper nanoporous structures for application to solar thermal heating

To elucidate the nanostructure impact on the light absorption and solar thermal heating performances, the carbonized nanopaper nanoporous structures were first tailored based on the workflow shown in **Figure 2a**. Cellulose nanofibers (width = 22 ± 8 nm) were prepared from never-dried softwood bleached kraft pulp by aqueous counter collision.[25] Subsequently, an aqueous cellulose nanofiber dispersion was dewatered, dried by hot pressing, treated with iodine (I_2), and then carbonized at 500 °C to produce an approximately 55-µm-thick carbonized nanopaper exhibiting dense structures (**Figures 2b and d**) because the cellulose nanofibers had aggregated during hot-press drying to evaporate high-surface-tension water (72.14 mN m^{-1} at 25 °C).[29] To suppress cellulose nanofiber aggregation, the water was exchanged for low-surface-tension (19.96 mN m^{-1} at 25 °C)[29] *tert*-butyl alcohol (*t*-BuOH) prior to freeze drying, the I_2 treatment, and then carbonizing the nanopaper. The as-prepared approximately 180-µm-thick carbonized nanopaper exhibited 3D nanoporous structures, which had been derived from the pore spaces between the layered cellulose nanofibers (**Figure 2c**). The nitrogen adsorption analysis using the Brunauer-Emmett-Teller (BET) theory and the Density Functional Theory (DFT) method indicated that the carbonized nanopaper exhibiting nanoporous structures contains mesopores (**Figure 2d**), while field-emission scanning electron microscopy (FE-SEM) images suggested that it also contains macropores smaller than approximately 100 nm (**Figure 2c**). The I_2 pretreatment was preformed to maintain the nanoporous structures of the nanopaper after carbonization, because the simple carbonization of the nanopaper deteriorates the morphology of cellulose nanofibers.[25] Although high-temperature treatment of cellulose removes carbon and hydrogen as a hydrocarbon gas and weakens its carbon frameworks, the I_2 pretreatment could overcome this problem; carbon removal during the high-temperature treatment was successfully suppressed by the I_2 treatment,[25] possibly owing to the preferential formation of HI.[30]

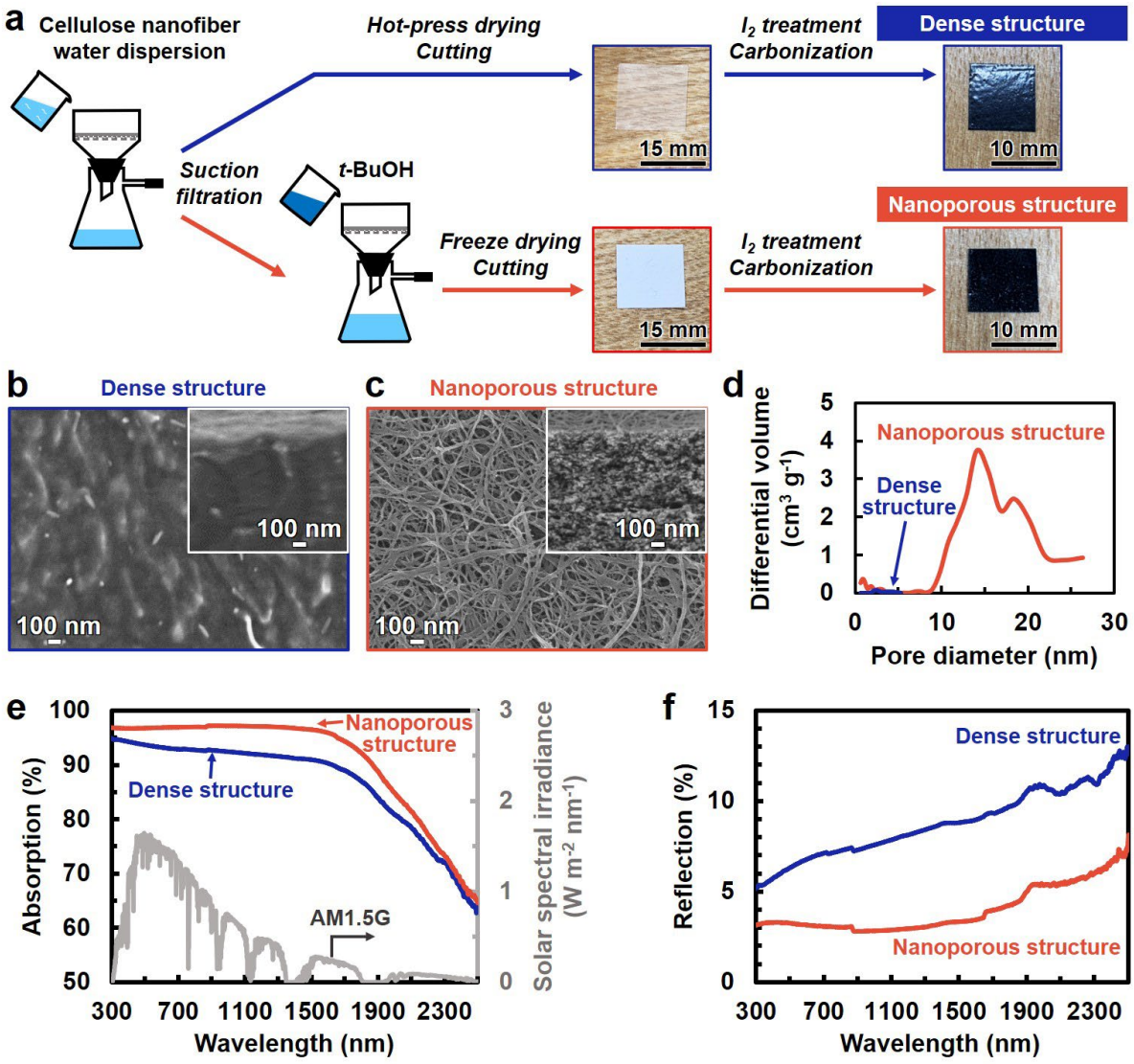

115

116 **Figure 2.** Preparation, porous structures, and light absorption properties of nanopapers
117 carbonized at 500 °C. (a) Preparation schematic and optical images, (b, c) cross-section (inset)
118 and surface field-emission scanning electron microscopy (FE-SEM) images, respectively, (d)
119 pore size distribution of carbonized nanopaper exhibiting dense or nanoporous structures, (e)
120 solar spectral irradiance (AM1.5G) and ultraviolet–visible–near infrared (UV–vis–NIR)
121 absorption, and (f) reflection of carbonized nanopaper exhibiting dense or nanoporous structures.

The carbonized nanopaper exhibiting the nanoporous structures showed greater light absorption (up to 97.2%) than that exhibiting the dense structures in the entire examined wavelength range (300–2500 nm), indicating that the nanoporous structures are beneficial for absorbing solar light (**Figure 2e**). As shown in **Figures 2a and f**, the dense structures gave the nanopaper a glossy appearance because of light reflecting off the structure surfaces. The nanoporous structures, on the other hand, gave the nanopaper a dark appearance by suppressing the light reflection (**Figures 2a and f**), albeit some light was transmitted at wavelengths above 1500 nm. Raman, X-ray diffraction (XRD), and Fourier-transform infrared (FT-IR) analyses suggested that the difference between the nanopaper molecular structures was negligible, regardless of whether the nanopaper exhibited dense or nanoporous structures (**Figure S1**). This result was possibly because the nanopapers had been carbonized at the same temperature. Thus, the nanoporous structures enhanced the carbonized nanopaper light absorption by suppressing the light reflection. These results indicated that the tailored carbonized nanopaper subwavelength nanoporous structures deserved the light confinement effect,[31] wherein the incident light is effectively captured owing to multiple light reflections and scattering in the nanopaper matrix.

Subsequently, the solar thermal heating performances of the carbonized nanopaper were evaluated under simulated solar light irradiation [AM1.5G, light intensity: 1.0 kW m^{-2} (1 sun)]. The change in surface temperature of the carbonized nanopaper irradiated under 1 sun was measured using a thermal camera (**Figure 3a**). The carbonized nanopaper temperature immediately increased upon 1 sun irradiation and saturated within 600 s (**Figure 3b**). Then, the equilibrium surface temperature of the carbonized nanopaper exhibiting the nanoporous structures reached 73.9 ± 0.80 °C, which was higher than that of the carbonized nanopaper exhibiting the dense structures (69.2 ± 0.65 °C). These results indicated that the nanoporous

structures gave the nanopaper superior solar thermal heating compared to the dense structures. Notably, the carbonized nanopaper exhibiting the tailored nanoporous structures also afforded higher light absorption and solar thermal heating performances than the carbonized cellulose pulp paper exhibiting porous microstructure derived from pulp-fiber-network-derived microscale pores (equilibrium surface temperature: 68.2 ± 0.96 °C) (**Figure S2**). Thus, designing subwavelength nanoporous structures in the carbonized nanopaper resulted in effective solar thermal heating by enhancing the solar absorption.

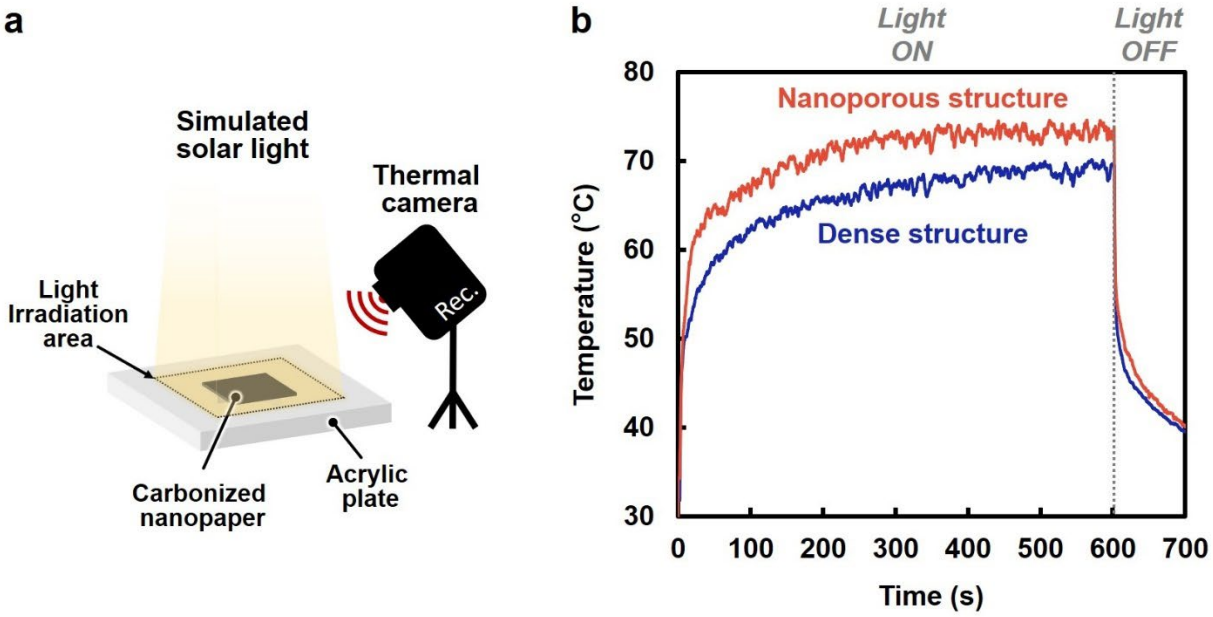

Figure 3. Photothermal heating performances of nanopapers (approximately 1 cm × 1 cm) carbonized at 500 °C and exhibiting different porous structures. (a) Schematic illustration of experimental setup used to measure surface temperature during simulated solar light irradiation, and (b) surface temperature evolutions measured under 1 sun irradiation for carbonized nanopapers exhibiting dense or nanoporous structures.

Solar thermal heating performances of nanopapers carbonized at different temperatures

Because the original nanopaper exhibiting nanoporous structures showed poor solar absorption and solar thermal heating (*e.g.*, the equilibrium surface temperature was only 37.9 °C for the nanopaper irradiated under 1 sun) (**Figure S3**), not only designing the subwavelength nanoporous structures but also carbonizing the nanopaper are the key to optimizing solar thermal heating. To elucidate the relationship between the nanopaper carbonization degree and the solar thermal heating performances, the nanopaper exhibiting nanoporous structures was carbonized in the temperature range of 300–1100 °C. The weight retention of the nanopaper was decreased from approximately 39.4 to 20.4% with increasing carbonization temperatures from 300 to 1100 °C, respectively (**Figure S4**). Then, the photothermal heating properties of the carbonized nanopapers were evaluated. As shown in **Figure 4a**, the photothermal heating performance of the carbonized nanopaper (1 cm × 1 cm, thickness = 160–200 μm) was dependent on carbonization temperature. Although the equilibrium surface temperature measured under 1 sun irradiation increased from 71.6 to 73.9 °C upon increasing carbonization temperature from 300 to 500 °C, respectively, it gradually decreased from 73.9 to 68.6 °C upon increasing carbonization temperature from 500 to 1100 °C, respectively. Thus, the nanopaper carbonized at 500 °C exhibited the best photothermal heating. According to the statistical analysis, the equilibrium surface temperature under 1 sun irradiation of the nanopaper carbonized at 500 °C was significantly different from those of the nanopapers carbonized at 300, 400, 600–1100 °C (p-value: ≤ 0.028).

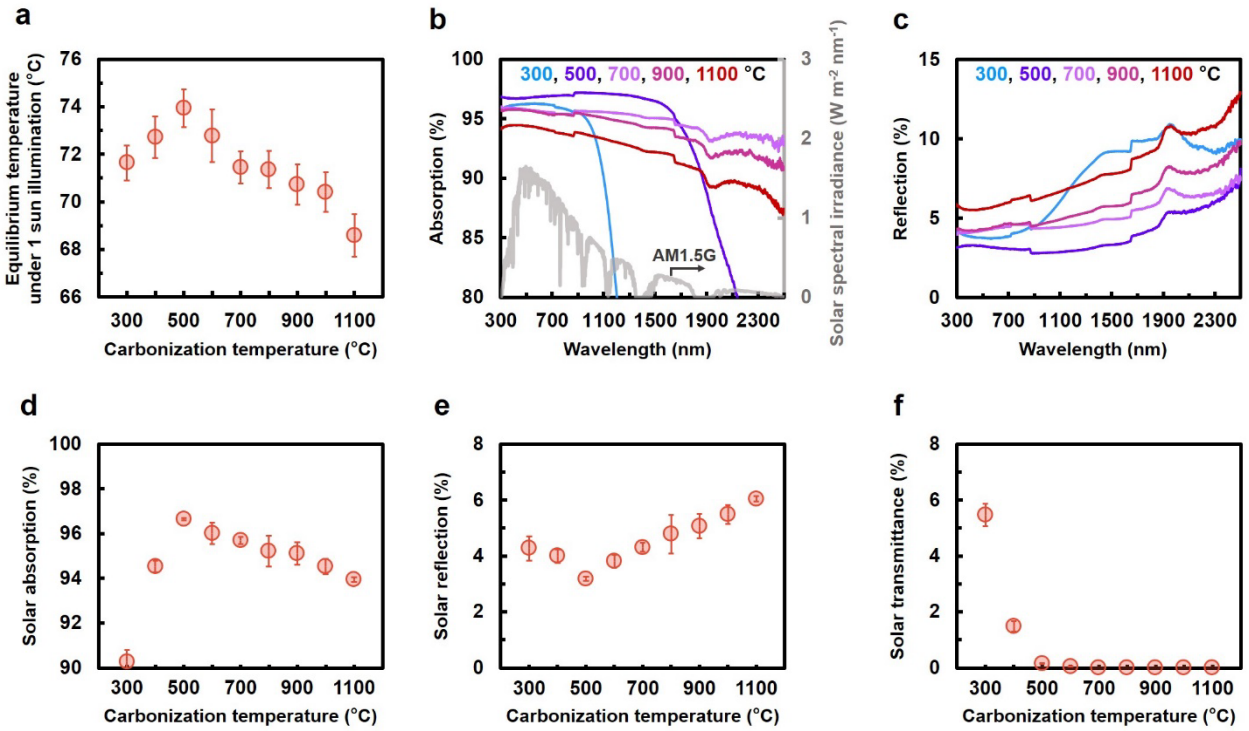

178

179 **Figure 4.** Photothermal heating and light absorption of nanopaper exhibiting nanoporous
180 structures carbonized at different temperatures. (a) Equilibrium surface temperature; (b) solar
181 spectral irradiance (AM1.5G) and UV–vis–NIR absorption; (c) reflection spectra; solar light (d)
182 absorption, (e) reflection, and (f) transmittance of nanopapers carbonized at different
183 temperatures.

184 To elucidate why the nanopaper carbonized at 500 °C exhibited the best photothermal
185 heating, the light absorption of the nanopapers carbonized at different temperatures were
186 compared (**Figure 4b**). With increasing carbonization temperature, the light absorption range of
187 the carbonized nanopaper extended toward the long-wavelength region. For instance, the
188 nanopapers carbonized above 700 °C exhibited over 90% light absorption across a broad
189 wavelength range. However, the nanopaper carbonized at 500 °C exhibited the highest light
190 absorption (up to 97.2%) in the wavelength range 300–1700 nm, which accounts for most solar

light energy. **Figure 4c** shows the light reflection of the nanopapers carbonized at different temperatures. The nanopaper carbonized at 300 °C exhibited relatively strong light reflection in the long-wavelength region (>1300 nm), where it also exhibited low light absorption. Notably, the nanopaper carbonized at 500 °C exhibited the lowest light reflection in the entire examined wavelength range (300–2500 nm), while the nanopapers carbonized above 500 °C exhibited increased light reflection.

To compare the solar absorptions of the nanopapers carbonized at different temperatures more clearly, the solar absorption was calculated according the following equation:[32]

$$\bar{\alpha} = \frac{\int_{\lambda_{min}}^{\lambda_{max}} I_{solar}(\lambda) \cdot \alpha_{solar}(\lambda) d\lambda}{\int_{\lambda_{min}}^{\lambda_{max}} I_{solar}(\lambda) d\lambda}, \quad (1)$$

where $\bar{\alpha}$ is the solar absorption (%), λ is the wavelength (nm), λ_{min} and λ_{max} are 300 and 2500 nm, respectively, $I_{solar}(\lambda)$ is the AM1.5G solar spectral irradiance at λ, and $\alpha_{solar}(\lambda)$ is the light absorption (%) at λ. Additionally, the solar reflection and transmittance were similarly calculated. **Figures 4d–f** show the as-calculated solar absorption, reflectance, and transmittance of the nanopapers carbonized at different temperatures. The nanopaper carbonized at 500 °C exhibited the highest solar absorption (96.7%) because it also exhibited the lowest solar reflectance (3.14%) and only a slight solar transmittance (0.16%). According to the statistical analysis, the solar absorption of the nanopaper carbonized at 500 °C was significantly different from those of the nanopapers carbonized at 300, 400, 600–1100 °C (p-value: ≤ 0.038). The solar absorption of nanopaper carbonized at 500 °C (96.7%) was superior to those of various carbonized biomass materials, such as carbonized mushroom (96%)[12], carbonized corncob (95.7%)[33], and arched bamboo charcoal (94.1%)[34]. Regardless of the carbonization temperature, the carbonized nanopapers exhibited almost no photoluminescence, indicating that most of the

213 solar light absorbed by the carbonized nanopaper had been converted to heat (**Figure S5**). These
214 results suggested that the nanopaper carbonized at 500 °C exhibited the best photothermal
215 heating (*i.e.*, the equilibrium surface temperature was 73.9 °C for the nanopaper irradiated under
216 1 sun; **Figure 4a**) because it exhibited excellent solar absorption by suppressing solar reflection.
217 The high surface temperature of the nanopaper carbonized at 500 °C and then irradiated under 1
218 sun was also attributed to the relatively low through-plane thermal conductivity (0.07 W m^{-1}
219 K^{-1}) (see **Figure S6** for more details). Thus, the nanopaper carbonized at 500 °C exhibited
220 excellent solar thermal heating and was also applied to solar-driven thermoelectric power
221 generation (**Figure S7**).

222 **Impact of carbonized nanopaper molecular structures on solar thermal heating**

223 Because the carbonized nanopaper nanoporous structures changed negligibly with the
224 carbonization temperature (**Figure S8**), the carbonization-temperature-dependent solar
225 absorption and thermal heating properties of the carbonized nanopaper were attributed to the
226 different cellulose nanofiber molecular structures formed at different carbonization temperatures.
227 To elucidate this point, during carbonization, the carbonized cellulose nanofiber molecular
228 structures were analyzed using FT-IR spectroscopy, Raman spectroscopy, XRD analysis, and
229 high-resolution transmission electron microscopy (HR-TEM). Although the original cellulose
230 molecule consists of sp^3-hybridized carbon structures, the FT-IR spectra indicated that sp^2-
231 hybridized carbon (C=C) and oxygen-containing functional groups such as C=O, C–O–C, and
232 C–OH had formed in the samples carbonized up to 500 °C (**Figure 5a**). The C=O, C–O–C, and
233 C–OH peaks weakened with increasing carbonization temperature. The C=C peak disappeared
234 from the spectra for the samples carbonized at or above 900 °C, suggesting that the π-conjugated
235 system had been extended because the sp^2-hybridized carbon domains had grown.[35] A G band

appeared in the Raman spectra of the samples carbonized at or above 500 °C, indicating that sp^2-hybridized graphitic carbon domains had formed (**Figure 5b**).[36] A D band also appeared, suggesting that the disordered graphitic carbon structures (*e.g.*, at the edge of the graphitic domains and in-plane imperfections)[36] remained even in the sample carbonized at 1100 °C.

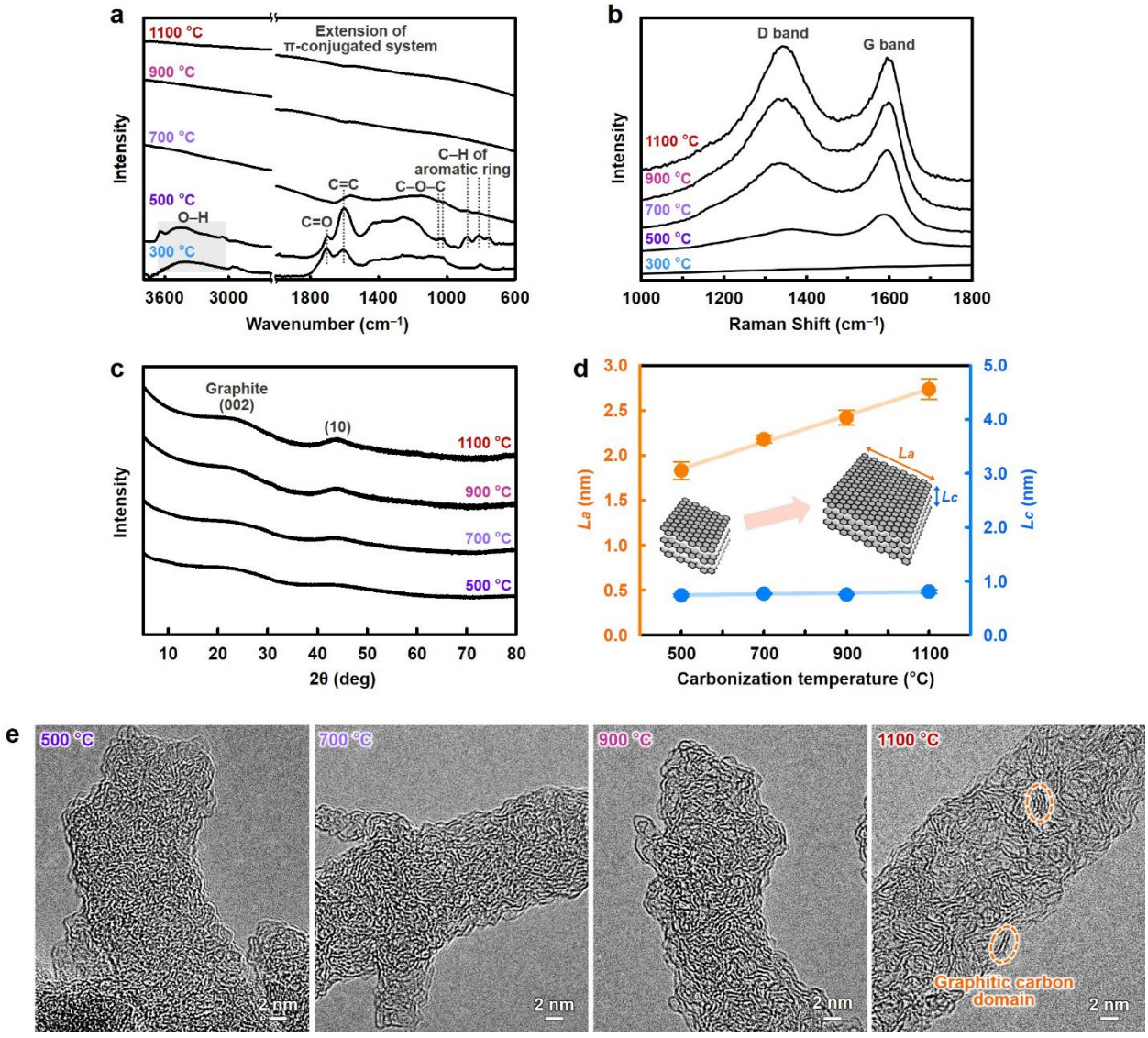

Figure 5. Molecular structural evolution of cellulose nanofibers during carbonization. (a) FT-IR, (b) Raman, and (c) XRD spectra; (d) graphitic carbon fragment crystallite sizes in in-plane (L_a)

and stacking (L_c) directions; and (e) HR-TEM images of cellulose nanofiber carbonized at different temperatures.

XRD was used to further analyze the sp^2-hybridized graphitic carbon domain growth during carbonization. As shown in **Figure 5c**, two broad peaks associated with the crystalline reflections (002) and the two-dimensional reflections (10) of graphite appeared at approximately 22° and 44°, corresponding to interplanar distances (d_c and d_a) of ~0.4 and ~0.2 nm, respectively[37]. These peaks intensified with increasing carbonization temperature. The graphite crystallite sizes in the stacking and in-plane directions (L_c and L_a, respectively) were estimated using these peaks and Scherrer's formula (**Figure 5d**).[37] Although L_c remained constant at ~1.0 nm, L_a gradually increased from ~1.8 to 2.7 nm upon increasing carbonization temperature from 500 to 1100 °C, suggesting that the graphitic carbon domains gradually grew in the in-plane rather than the stacking direction. These trends were consistently observed in the corresponding HR-TEM images (**Figure 5e**). Notably, numerous randomly oriented graphitic carbon domains exhibiting layer structures with the width and thickness of a few nanometers more prominently appeared at higher carbonization temperatures, which confirmed that graphitic carbon domains had progressively grown in the carbonized cellulose nanofiber with increasing carbonization temperature.

Such progressive graphitic carbon domain growth governed the carbonization-temperature-dependent solar absorption and thermal heating of the nanopaper as follows. The original nanopaper exhibited poor solar absorption (**Figure S3**) owing to the wide σ–σ^* energy gap of the sp^3-hybridized carbons in the cellulose molecule. The nanopaper carbonized at 300 °C exhibited sp^2-hybridized carbon domains (*i.e.*, π-orbitals), wherein the π–π^* energy gap is within

the σ–σ* one[38] and promotes light absorption at lower energies (*i.e.*, longer wavelengths) than the original nanopaper. In the nanopapers carbonized at temperatures of 500 °C or above, the light-absorption wavelength range can be further extended to longer wavelengths by growing graphitic sp^2-hybridized carbon domains (**Figure 4b**) because the π–π^* energy gap decreases with the growth of these domains[38]. However, excess sp^2-hybridized graphitic carbon domain growth increases light reflection across a broad wavelength range (**Figure 4c**). Such light reflection would be associated with graphitic-carbon-domain-induced metallic luster, as previously reported for graphite films,[39] graphene nanosheets,[40] and graphene papers.[41] To effectively absorb solar irradiation, therefore, the graphitic carbon domain growth should be tailored to extend the light-absorption wavelength range while suppressing the light reflection. In this study, the nanopaper carbonized at 500 °C exhibited this optimal balance; the graphitic carbon domains therein exhibited an L_c and L_a of ~0.74 and 1.83 nm, respectively (**Figure 5d**). Such semicarbonized cellulose molecular structures provided the highest solar absorption (96.7%) and the lowest solar reflectance (3.14%) (**Figures 4d** and **e**, respectively); therefore, the nanopaper carbonized at 500 °C exhibited the best solar thermal heating (**Figure 4a**). Furthermore, the low through-plane thermal conductivity of the semicarbonized nanopaper (0.07 W m^{-1} K^{-1}) (**Figure S6**) can be beneficial for localized heating[42], providing a higher surface temperature for the nanopaper irradiated under 1 sun than even state-of-the-art nanocarbon materials, such as a carbon nanotube black body, graphene paper, and graphene oxide film (**Table 1**). Such higher surface temperature can contribute to the effective use of renewable solar energy such as solar-driven thermoelectric power generation. For example, Komatsu et al. has recently reported the macroscopic weavable fibers of carbon nanotubes with giant thermoelectric power factor (14 mW m^{-1} K^{-2})[43], indicating that even a 1 K temperature difference can produce

mW levels of energy. Thus, the excellent solar thermal heating performance of the semicarbonized nanopaper exhibiting nanoporous structures can be significant toward the effective use of renewable solar energy.

Table 1. Photothermal heating performances of nanopaper semicarbonized at 500 °C and various conventional carbon materials irradiated under 1 sun.

Carbon material	Surface temperature (°C)
CNT† black body	55.0 ± 0.28
Graphite sheet	64.5 ± 1.98
Graphene paper	65.2 ± 1.46
Graphene oxide film	69.4 ± 1.53
Semicarbonized nanopaper exhibiting nanoporous structures	73.9 ± 0.80

†CNT, carbon nanotube.

CONCLUSION

In summary, a semicarbonized cellulose nanofiber paper was tailored with subwavelength nanoporous structures and adequately grown graphitic carbon domains for application to solar thermal heating. The tailored subwavelength nanoporous structures enhanced

the solar absorption by suppressing the light reflection. The graphitic carbon domains grown by semicarbonization at 500 °C balanced the tradeoff between extending the light-absorption wavelength range and suppressing the light reflection. Thus, the semicarbonized subwavelength-nanopore-structured nanopaper exhibited high solar absorption, and therefore, effective solar thermal heating, which enabled the nanopaper to be applied to thermoelectric power generation. While a further challenge remains to make the tailoring process of the nanoporous structures greener, the study findings can provide a guideline for structurally designing biomass-derived carbon materials for application to solar absorption and thermal heating. Furthermore, the concept for tailoring the carbonized cellulose nanofiber nanoporous and molecular structures can be applied to various carbonized bionanomaterials, opening a pathway to develop structurally and functionally designable carbonized bionanomaterials for diverse applications.

EXPERIMENTAL SECTION

Materials

According to the method detailed in our previous report,[25] never-dried softwood bleached kraft pulp and a high-pressure water-jet system equipped with a counter-collision chamber (Star Burst, HJP-25005E, Sugino Machine Co., Ltd., Uozu, Japan) were used to prepare a cellulose nanofiber/water dispersion. Briefly, the pulp suspension was ejected from a ⌀0.12-mm nozzle at 245 MPa for 100 passes. Iodine (>99.8% purity) and *tert*-butyl alcohol (*t*-BuOH, >99.0% purity) were purchased from Nacalai Tesque, Inc., Kyoto, Japan. A CNT black body was obtained from MICROPHASE Co., Ltd., Tsukuba, Japan. A graphite sheet (EYGS121810) was purchased from Panasonic Corp., Osaka, Japan. A graphene paper (900451-1EA) and a graphene oxide film (798991-1EA) were obtained from Merck KGaA, Darmstadt, Germany.

Nanopaper preparation and carbonization

The nanopaper was prepared and carbonized according to the method detailed in our previous report.[25] Briefly, a cellulose nanofiber/water dispersion (0.2 wt.%, 200 mL) was suction filtered through a hydrophilic polytetrafluoroethylene (PTFE) filter (H020A090C, pore diameter of 0.2 μm, Toyo Roshi Kaisha, Ltd., Tokyo, Japan), rinsed with *t*-BuOH (200 mL), and suction filtered again. The wet sheet was peeled off the PTFE filter, immersed in liquid nitrogen for 1 min, and freeze-dried (EYELA, FDU-2200, Tokyo Rikakikai Co., Ltd., Tokyo, Japan) overnight to prepare a nanopaper exhibiting a nanoporous structure. A nanopaper exhibiting a dense structure was prepared without using any *t*-BuOH by hot pressing at 110 °C and 1.1 MPa for 30 min (AYSR-5, Shinto Metal Industries, Ltd., Osaka, Japan). Porous-microstructured cellulose pulp paper was similarly prepared using *t*-BuOH by hot pressing. Prior to carbonization, the nanopaper and pulp paper were treated with I_2 gas (the same weight as the paper) at 100 °C for 24 h in a sealed flask to retain the original morphology during carbonization.[25] The I_2-treated papers were then carbonized in a furnace (KDF-75, DENKEN-HIGHDENTAL Co., Ltd., Kyoto, Japan) in three stages under nitrogen flowing at 500 mL min^{-1}, while removing the generated corrosive HI gas in the furnace. First, the temperature was increased at 2 °C min^{-1} from room temperature to 240 °C and was maintained there for 17 h. This treatment is also effective to avoid destruction of the original fibrous morphology during carbonization.[44] Then, the temperature was increased at 2 °C min^{-1} to peak carbonization temperatures in the range 300–1100 °C and was maintained there for 1 h. Finally, the nanopaper was cooled at 2 °C min^{-1} to room temperature. Regardless of the peak carbonization temperature, the dimensions of the carbonized papers were set at approximately 1 cm × 1 cm by adjusting the original paper size.

Nanopaper thermal heating performance evaluated under solar light irradiation

The solar thermal heating performances of the carbonized nanopaper were evaluated by measuring the nanopaper surface temperatures under solar light irradiation, according to a method detailed in our previous report.[45] Prior to the temperature measurements, the emissivity of each nanopaper was evaluated using black body tape exhibiting an emissivity of 0.95 (HB-250, OPTEX Co., Ltd., Shiga, Japan) as a reference. The nanopaper and black tape were heated using a temperature controller (SBX-303, Sakaguchi E.H. VOC Corp., Tokyo, Japan) to 75 °C. The nanopaper emissivity was estimated by adjusting the nanopaper temperature measured using an infrared thermal camera (FLIR ETS320, FLIR Systems, Inc., Wilsonville, USA) according to the black tape reference temperature. For the surface temperature measurements, a solar simulator (AM1.5G, HAL-320W, Asahi Spectra Co., Ltd., Tokyo, Japan) was used as the light source. The samples (1 cm × 1 cm) were put on an acrylic plate (3 cm × 3 cm) exhibiting a central hole (0.7 cm × 0.7 cm), and the surface temperature changes of the samples illuminated using the solar simulator (light intensity: 1 sun) were recorded using the infrared thermal camera according to the nanopaper-calibrated emissivity. The equilibrium surface temperature of the samples was calculated as the average surface temperature during 1 sun-irradiation time of 500–600 s (approximately 850 plots). For data reproducibility and statistical analyses, more than 6 samples were prepared for each condition; a p value less than 0.05 was considered statistically significant. The solar thermal heating performance was measured at 25 °C and 65% relative humidity. The CNT black body, graphite sheet, graphene paper, and graphene oxide film solar thermal heating performances were similarly evaluated for comparison.

Nanopaper application to solar-driven thermoelectric power generation

The nanopaper (3.5 cm × 3.5 cm) carbonized at 500 °C was attached to a commercial thermoelectric power generator (4.0 cm × 4.0 cm, 66900, Artec Co., Ltd., Osaka, Japan) using a

heat-dissipation adhesive (COM-G52, COM Institute, Inc., Osaka, Japan) to fabricate a thermoelectric power generation module, three of which were integrated into one solar-driven thermoelectric power generation device. A propeller motor (P70-3935, working voltage and current ranges of 0.4–1.5 V and 16–20 mA, respectively, Narika Corp., Tokyo, Japan) was used to generate electrical energy. On a sunny day (October 21, 2020; 24.5 °C, 34°49′30″ N, 135°31′28″ E), natural sunlight was irradiated on one side of the nanopaper carbonized at 500 °C while the other side was cooled using an ice pack.

Characterization

The nanopaper surface morphology was observed using FE-SEM (SU-8020, Hitachi High-Tech Science Corp., Tokyo, Japan) at an accelerate voltage of 2 kV to avoid damage to the nanofibers. The pore size distribution was evaluated at 77 K based on nitrogen adsorption analysis using the BET theory and the DFT method (NOVA 4200e, Quantachrome Instruments, Kanagawa, Japan). The light transmittance, reflectance, and absorption were measured using UV–vis–NIR spectroscopy (UV-3600i Plus, Shimadzu Corporation, Kyoto, Japan) with an integrating sphere attachment (ISR-603, Shimadzu Corp., Kyoto, Japan). Absorption spectra were calculated from total transmittance and total reflectance spectra. For data reproducibility and statistical analyses, more than 6 samples were prepared for each condition; a p value less than 0.05 was considered statistically significant. The FT-IR (KJP-05120S, PerkinElmer Japan Co., Ltd., Kanagawa, Japan) spectra were recorded in attenuated total reflection (ATR) mode. The Raman spectra were recorded using a RAMAN-touch apparatus (Nanophoton Corp., Osaka, Japan) and a 532-nm incident laser. To analyze the carbon fragment crystal structures, the XRD (Ultima IV, Rigaku Corporation, Tokyo, Japan) spectra were recorded using Ni-filtered Cu-Kα radiation (1.5418 Å), and the nanopapers were scanned in the range $2\theta = 5–80°$ at 30-kV

acceleration and 40 mA. The graphitic carbon fragment crystallite sizes in the stacking (L_c) and in-plane (L_a) directions were estimated using the XRD spectra and the Scherrer formula $L = k\lambda/\beta\cos\theta$, where λ, β, and θ are the X-ray wavelength, full width at half maximum, and Bragg angle, respectively. L_c and L_a were estimated using the crystalline reflections (002) and the two-dimensional reflections (10) with $k = 0.89$ and 1.84, respectively, according to the method described in a previous report.[37] HR-TEM (JEM-ARM 200F, JEOL Ltd., Tokyo, Japan) observation was operated at 200 kV. The photoluminescence spectra were recorded using a Quantaurus-QY instrument (C11347-01, HAMAMATSU PHOTONICS K. K., Shizuoka, Japan). The nanopaper thermal conductivity was calculated based on the following equation:

$$K = \alpha \cdot \rho \cdot C_p, \qquad (2)$$

where K, α, ρ, and C_p indicate the nanopaper thermal conductivity (W m^{-1} K^{-1}), thermal diffusivity (mm^2 s^{-1}), density (g cm^{-3}), and specific heat capacity (J g^{-1} K^{-1}), respectively. The through-plane thermal diffusivity (α) was measured using a light flash apparatus (LFA447 HyperFlash, NETZSCH, Selb, Germany). The specific heat capacity (C_p) was measured using differential scanning calorimetry (Thermo Plus EVO II, Rigaku Corp., Tokyo, Japan). Al_2O_3 was used as a reference, and the thermograms were generated by heating the nanopapers at 10 °C min^{-1} in the temperature range 0–110 °C in a N_2 atmosphere.[46]

ASSOCIATED CONTENT

Supporting Information

The following files are available free of charge upon reasonable request from the corresponding author or on the Internet at http://pubs.acs.org.

Molecular structures of carbonized nanopapers exhibiting nanoporous and dense structures

(PDF)

Porous structures, light absorption and reflection measurements, and solar thermal heating performances of cellulose pulp paper carbonized at 500 °C exhibiting porous microstructures (PDF)

UV–vis–NIR absorption spectrum of original nanopaper (PDF)

Weight retention of nanopaper carbonized at different temperatures (PDF)

Carbonized nanopaper photoluminescence spectra (PDF)

Carbonized nanopaper thermal property measurements (PDF)

Solar-driven thermoelectric power generation using carbonized nanopaper (PDF)

Nanoporous structures of nanopapers carbonized at different temperatures (PDF)

AUTHOR INFORMATION

Corresponding Author

*Hirotaka Koga

SANKEN (The Institute of Scientific and Industrial Research), Osaka University, 8-1 Mihogaoka, Ibaraki, Osaka 567-0047, Japan

Phone: +81-6-6879-8442; Fax: +81-6-6879-8444; E-mail: hkoga@eco.sanken.osaka-u.ac.jp

ORCIDs

Thanakorn Yeamsuksawat: 0000-0003-2363-6426

Yintong Huang: 0000-0001-7385-0661

Takaaki Kasuga: 0000-0002-3576-943X

Hirotaka Koga: 0000-0001-6295-1731

Author Contributions

The manuscript was written through contributions of all the authors, who have approved the final manuscript version.

H. Koga designed the study. T. Yeamsuksawat and H. Koga wrote the manuscript. T. Yeamsuksawat and Y. Morishita prepared the samples. T. Yeamsuksawat, Y. Morishita, J. Shirahama, and Y. Huang performed the experiments. T. Yeamsuksawat, Y. Morishita, J. Shirahama, Y. Huang, T. Kasuga, M. Nogi, and H. Koga analyzed the results, discussed the results and implications, and commented on the manuscript at all the preparation stages.

Notes

The authors declare no competing financial interests.

ACKNOWLEDGMENT

This work was partially supported by Grants-in-Aid for Scientific Research (Grant No. 20K21334 to H. K.) from the Japan Society for the Promotion of Science, JST FOREST Program (Grant No. JPMJFR2003 to H. K.), "Nanotechnology Platform Project (Nanotechnology Open Facilities in Osaka University)" of the Ministry of Education, Culture, Sports, Science, and Technology (MEXT), Japan (No. JPMXP09S21OS0029 to H. K.), MEXT Project for promoting the public utilization of advanced research infrastructure (Program for supporting the construction of core facilities) (Grant No. JPMXS0441200021), and JICA Innovative Asia program 4th Batch (Grant No. 201905897J023 to T. Y.). We thank the members of the Comprehensive Analysis Center and the Flexible 3D System Integration Laboratory, SANKEN, Osaka University, for assistance with HR-TEM imaging and thermal conductivity measurements, respectively.

ABBREVIATIONS

ATR, attenuated total reflection; CNT, carbon nanotube; FE-SEM, field-emission scanning electron microscopy; FT-IR, Fourier-transform infrared; HR-TEM, high-resolution transmission electron microscopy; NIR, near infrared; PL, photoluminescence; PTFE, polytetrafluoroethylene; TEM, transmission electron microscopy; *t*-BuOH, *tert*-butyl alcohol; UV, ultraviolet; vis, visible; XRD, X-ray diffraction.

REFERENCES

(1) Szczęśniak, B.; Phuriragpitikhon, J.; Choma, J.; Jaroniec, M. Recent Advances in the Development and Applications of Biomass-Derived Carbons with Uniform Porosity. *J. Mater. Chem. A* **2020**, *8*, 18464–18491.

(2) Wang, Y.; Zhang, M.; Shen, X.; Wang, H.; Wang, H.; Xia, K.; Yin, Z.; Zhang, Y. Biomass-Derived Carbon Materials: Controllable Preparation and Versatile Applications. *Small* **2021**, *17*, 2008079.

(3) Jiao, G.-J.; Ma, J.; Li, Y.; Jin, D.; Ali, Z.; Zhou, J.; Sun, R. Recent Advances and Challenges on Removal and Recycling of Phosphate from Wastewater Using Biomass-Derived Adsorbents. *Chemosphere* **2021**, *278*, 130377.

(4) Konwar, L. J.; Boro, J.; Deka, D. Review on Latest Developments in Biodiesel Production Using Carbon-Based Catalysts. *Renew. Sust. Energ. Rev.* **2014**, *29*, 546–564.

(5) Wang, C.; Xia, K.; Wang, H.; Liang, X.; Yin, Z.; Zhang, Y. Advanced Carbon for Flexible and Wearable Electronics. *Adv. Mater.* **2019**, *31*, 1801072.

(6) Zhu, L.; Huang, Y.; Morishita, Y.; Uetani, K.; Nogi, M.; Koga, H. Pyrolyzed Chitin Nanofiber Paper as a Three-Dimensional Porous and Defective Nanocarbon for Photosensing and Energy Storage. *J. Mater. Chem. C* **2021**, *9*, 4444–4452.

(7) Deng, J.; Li, M.; Wang, Y. Biomass-Derived Carbon: Synthesis and Applications in Energy Storage and Conversion. *Green Chem.* **2016**, *18*, 4824–4854.

(8) Zhu, L.; Uetani, K.; Nogi, M.; Koga, H. Polydopamine Doping and Pyrolysis of Cellulose Nanofiber Paper for Fabrication of Three-Dimensional Nanocarbon with Improved Yield and Capacitive Performances. *Nanomaterials* **2021**, *11*, 3249.

(9) Zhang, C.; Liang, H.; Xu, Z.; Wang, Z. Harnessing Solar-Driven Photothermal Effect toward the Water–Energy Nexus. *Adv. Sci.* **2019**, *6*, 1900883.

(10) Liu, H.; Chen, C.; Chen, G.; Kuang, Y.; Zhao, X.; Song, J.; Jia, C.; Xu, X.; Hitz, E.; Xie, H.; Wang, S.; Jiang, F.; Li, T.; Li, Y.; Gong, A.; Yang, R.; Das, S.; Hu, L. High-Performance Solar Steam Device with Layered Channels: Artificial Tree with a Reversed Design. *Adv. Energy Mater.* **2018**, *8*, 1701616.

(11) Wu, X.; Wu, L.; Tan, J.; Chen, G. Y.; Owens, G.; Xu, H. Evaporation above a Bulk Water Surface Using an Oil Lamp Inspired Highly Efficient Solar-Steam Generation Strategy. *J. Mater. Chem. A* **2018**, *6*, 12267–12274.

(12) Xu, N.; Hu, X.; Xu, W.; Li, X.; Zhou, L.; Zhu, S.; Zhu, J. Mushrooms as Efficient Solar Steam-Generation Devices. *Adv. Mater.* **2017**, *29*, 1606762.

(13) Liu, J.; Liu, Q.; Ma, D.; Yuan, Y.; Yao, J.; Zhang, W.; Su, H.; Su, Y.; Gu, J.; Zhang, D. Simultaneously Achieving Thermal Insulation and Rapid Water Transport in Sugarcane Stems for Efficient Solar Steam Generation. *J. Mater. Chem. A* **2019**, *7*, 9034–9039.

(14) Zhu, M.; Yu, J.; Ma, C.; Zhang, C.; Wu, D.; Zhu, H. Carbonized Daikon for High Efficient Solar Steam Generation. *Sol. Energy Mater. Sol. Cells* **2019**, *191*, 83–90.

(15) Villabona-Leal, E. G.; Escobar-Villanueva, A. G.; Pérez-Pérez, E. B.; Martínez-Gutiérrez, H.; Ovando-Medina, V. M. Efficient Photothermal Supports from Carbonized Agave Flower Stalk for Solar Water Evaporation. *Int. J. Energy Res.* **2021**, *45*, 19521–19534.

(16) Gao, M.; Zhu, L.; Peh, C. K.; Ho, G. W. Solar Absorber Material and System Designs for Photothermal Water Vaporization towards Clean Water and Energy Production. *Energy Environ. Sci.* **2019**, *12*, 841–864.

(17) ASTM G173-03. Standard Tables for Reference Solar Spectral Irradiances: Direct Normal and Hemispherical on 37° Tilted Surface; ASTM International: West Conshohocken, PA, 2012.

(18) Zheng, X.; Zhang, L. Photonic Nanostructures for Solar Energy Conversion. *Energy Environ. Sci.* **2016**, *9*, 2511–2532.

(19) Feng, G.; Zhang, G.-Q.; Ding, D. Design of Superior Phototheranostic Agents Guided by Jablonski Diagrams. *Chem. Soc. Rev.* **2020**, *49*, 8179–8234.

(20) Thomas, B.; Raj, M. C.; B, A. K.; H, R. M.; Joy, J.; Moores, A.; Drisko, G. L.; Sanchez, C. Nanocellulose, a Versatile Green Platform: From Biosources to Materials and Their Applications. *Chem. Rev.* **2018**, *118*, 11575–11625.

(21) Isogai, A.; Saito, T.; Fukuzumi, H. TEMPO-Oxidized Cellulose Nanofibers. *Nanoscale* **2011**, *3*, 71–85.

(22) Moon, R. J.; Martini, A.; Nairn, J.; Simonsen, J.; Youngblood, J. Cellulose Nanomaterials Review: Structure, Properties and Nanocomposites. *Chem. Soc. Rev.* **2011**, *40*, 3941.

(23) *Nanocellulose Market by Type (MFC & NFC, CNC/NCC), Raw Material (Wood, Non-Wood), Application (Pulp & Paper, Composites, Biomedical & Pharmaceuticals, Electronics & Sensors), and region (North America, APAC, Europe, RoW) - Global Forecast to 2026*; Research and Markets: Dublin, Ireland, **2022**.

(24) Klemm, D.; Heublein, B.; Fink, H.-P.; Bohn, A. Cellulose: Fascinating Biopolymer and Sustainable Raw Material. *Angew. Chem. Int. Ed.* **2005**, *44*, 3358–3393.

(25) Koga H; Nagashima K; Suematsu K; Takahashi T; Zhu L; Fukushima D; Huang Y; Nakagawa R; Liu J; Uetani K; Nogi M; Yanagida T; Nishina T. Nanocellulose Paper Semiconductor with a 3D Network Structure and Its Nano–Micro–Macro Trans-Scale Design. *ACS Nano* **2022**, *16*, 8630–8640.

(26) Liang, H.-W.; Guan, Q.-F.; Zhu, Z.-; Song, L.-T.; Yao, H.-B.; Lei, X.; Yu, S.-H. Highly Conductive and Stretchable Conductors Fabricated from Bacterial Cellulose. *NPG Asia Mater.* **2012**, *4*, e19–e19.

(27) Wu, Z.-Y.; Liang, H.-W.; Chen, L.-F.; Hu, B.-C.; Yu, S.-H. Bacterial Cellulose: A Robust Platform for Design of Three Dimensional Carbon-Based Functional Nanomaterials. *Acc. Chem. Res.* **2016**, *49*, 96–105.

(28) Li, S.-C.; Hu, B.-C.; Ding, Y.-W.; Liang, H.-W.; Li, C.; Yu, Z.-Y.; Wu, Z.-Y.; Chen, W.-S.; Yu, S.-H. Wood-Derived Ultrathin Carbon Nanofiber Aerogels. *Angew. Chem. Int. Ed.* **2018**, *57*, 7085–7090.

(29) Jasper, J. J. The Surface Tension of Pure Liquid Compounds. *J. Phys. Chem. Ref. Data* **1972**, *1*, 841–1010.

(30) Kyotani, M.; Matsushita, S.; Nagai, T.; Matsui, Y.; Shimomura, M.; Kaito, A.; Akagi, K. Helical Carbon and Graphitic Films Prepared from Iodine-Doped Helical Polyacetylene Film Using Morphology-Retaining Carbonization. *J. Am. Chem. Soc.* **2008**, *130*, 10880−10881.

(31) Wang, J.; Zhao, J.; Li, Y.; Yang, M.; Chang, Y.-Q.; Zhang, J.-P.; Sun, Z.; Wang, Y. Enhanced Light Absorption in Porous Particles for Ultra-NIR-Sensitive Biomaterials. *ACS Macro Lett.* **2015**, *4*, 392–397.

(32) Mandal, J.; Wang, D.; Overvig, A. C.; Shi, N. N.; Paley, D.; Zangiabadi, A.; Cheng, Q.; Barmak, K.; Yu, N.; Yang, Y. Scalable, "Dip-and-Dry" Fabrication of a Wide-Angle Plasmonic Selective Absorber for High-Efficiency Solar–Thermal Energy Conversion. *Adv. Mater.* **2017**, *29*, 1702156.

(33) Chen, Y.; Sha, C.; Yu, Y.; Wang, W. A Simple, Scalable, Low-Cost Honeycomb-Like Carbonized Corncob for Highly Efficient Solar Steam Generation. *Adv. Sustainable Syst.* **2022**, *6*, 2100300.

(34) Li, Z.; Wang, C.; Lei, T.; Ma, H; Su, J.; Ling, S.; Wang, W. Arched Bamboo Charcoal as Interfacial Solar Steam Generation Integrative Device with Enhanced Water Purification Capacity. *Adv. Sustainable Syst.* **2019**, *3*, 1800144.

(35) Ning, J.; Hao, L.; Jin, M.; Qiu, X.; Shen, Y.; Liang, J.; Zhang, X.; Wang, B.; Li, X.; Zhi, L. A Facile Reduction Method for Roll-to-Roll Production of High Performance Graphene-Based Transparent Conductive Films. *Adv. Mater.* **2017**, *29*, 1605028.

(36) Dresselhaus, M. S.; Jorio, A.; Souza Filho, A. G.; Saito, R. Defect Characterization in Graphene and Carbon Nanotubes Using Raman Spectroscopy. *Philos. Trans. Royal Soc. A* **2010**, *368*, 5355–5377.

(37) Biscoe, J.; Warren, B. E. An X-Ray Study of Carbon Black. *J. Appl. Phys.* **1942**, *13*, 364–371.

(38) Mathioudakis, C.; Kopidakis, G.; Kelires, P. C.; Patsalas, P.; Gioti, M.; Logothetidis, S. Electronic and Optical Properties of A-C from Tight-Binding Molecular Dynamics Simulations. *Thin Solid Films* **2005**, *482*, 151–155.

(39) Isayama, M.; Nomiyama, K.; Kunitake, T. Template Synthesis of a Large, Self-Supporting Graphite Film in Montmorillonite. *Adv. Mater.* **1996**, *8*, 641–644.

(40) Li, D.; Müller, M. B.; Gilje, S.; Kaner, R. B.; Wallace, G. G. Processable Aqueous Dispersions of Graphene Nanosheets. *Nat. Nanotechnol.* **2008**, *3*, 101–105.

(41) Chen, H.; Müller, M. B.; Gilmore, K. J.; Wallace, G. G.; Li, D. Mechanically Strong, Electrically Conductive, and Biocompatible Graphene Paper. *Adv. Mater.* **2008**, *20*, 3557–3561.

(42) Yang, Y.; Yang, X.; Fu, L.; Zou, M.; Cao, A.; Du, Y.; Yuan, Q.; Yan, C.-H. Two-Dimensional Flexible Bilayer Janus Membrane for Advanced Photothermal Water Desalination. *ACS Energy Lett.* **2018**, *3*, 1165–1171.

(43) Komatsu, N.; Ichinose, Y.; Dewey, O. S.; Taylor, L. W.; Trafford, M. A.; Yomogida, Y.; Wehmeyer, G.; Pasquali, M.; Yanagi, K.; Kono, J. Macroscopic Weavable Fibers of Carbon Nanotubes with Giant Thermoelectric Power Factor. *Nat. Commun.* **2021**, *12*, 4931.

(44) Jazaeri, E.; Tsuzuki, T. Effect of Pyrolysis Conditions on the Properties of Carbonaceous Nanofibers Obtained from Dreeze-Dried Cellulose Nanofibers. *Cellulose* **2013**, *20*, 707–716.

(45) Huang, Y.; Morishita, Y.; Uetani, K.; Nogi, M.; Koga, H. Cellulose Paper Support with Dual-Layered Nano–Microstructures for Enhanced Plasmonic Photothermal Heating and Solar Vapor Generation. *Nanoscale Adv.* **2020**, *2*, 2339–2346.

(46) Meng, X.; Pan, H.; Zhu, C.; Chen, Z.; Lu, T.; Xu, D.; Li, Y.; Zhu, S. Coupled Chiral Structure in Graphene-Based Film for Ultrahigh Thermal Conductivity in Both In-Plane and Through-Plane Directions. *ACS Appl. Mater. Interfaces* **2018**, *10*, 22611–22622.

590 TOC GRAPHIC

591